34th Space Symposium, Technical Track, Colorado Springs, Colorado, United States of America
Presented on April 16, 2018

WAVEFRONT SENSING AND CONTROL FOR THE JAMES WEBB SPACE TELESCOPE

D. Scott Acton
Ball Aerospace and Technologies Corporation. dsacton@ball.com.

Bruce Dean, Lee Feinberg
NASA Goddard Space Flight Center.

Marshal Perrin, Charles Lajoie, Matthew Lallo
Space Telescope Science Institute.

ABSTRACT

The James Webb Space Telescope (JWST) is a segmented deployable telescope, utilizing 6 degrees of freedom for adjustment of the Secondary Mirror (SM) and 7 degrees of freedom for adjustment of each of its 18 segments in the Primary Mirror (PM). When initially deployed, the optical elements will be positioned to within a few mm of their nominal positions. The Wavefront Sensing and Controls (WFSC) process will position the optical elements to within a few nm, resulting in a diffraction-limited telescope across the entire science field. It relies primarily on normal imaging modes of the science instrumentation, and special optical elements placed in the internal filter wheel of the Near Infrared Camera (NIRCam). The WFSC process has benefited from 15 years of development and is now ready to be applied on the JWST in flight. This paper will describe the WFSC process algorithms and software. The results of flight-like end-to-end simulations showing the commissioning process will also be presented.

1. INTRODUCTION

The most unique aspect of performing Wavefront Sensing and Control (WFSC) on JWST is that the observatory does not contain an actual wavefront sensor. The Near-Infrared Camera (NIRCam) [1], however, has been designed with wavefront sensing in mind. The plate scale of NIRCam allows for critically-sampled images, at λ=2μm. It supports a pupil imaging mode for establishing pupil constraints and for diagnostics. Eight of NIRCam's 48 filter wheel positions contain hardware specifically to support WFSC. Finally, the NIRCam instrument actually consists of two independent and fully-redundant modules, each capable of supporting WFSC. The majority of the WFSC activities take place in NIRCam. The other science instruments on JWST are used to measure the field-dependent wavefront errors (section 2.10).

The observatory has been designed to rely on passive stability. As such, the WFSC is not performed automatically. Exposures taken by science instruments are sent from the Observatory through the Deep Space Network to the Science and Operations Center (SOC). Within the SOC, initial processing of both science and engineering data is performed by the Flight Operations Subsystem (FOS), which forwards the science data to the Data Management Subsystem (DMS) [2]. The DMS reformats, calibrates, and assembles individual exposures into science-quality images. The DMS then forwards the images to the Wavefront Sensing and Control Software Subsystem (WSS). The WSS is an SOC subsystem with three components: The WSS Executive (WEx) [3], the Wavefront Analysis Software (WAS) and the Mirror Control Software (MCS). The WEx provides the interface to the SOC and allows the wavefront scientist to control the WAS and MCS, review previous sessions and examine the current state of the mirror segments. The WEx invokes the WAS to perform wavefront processing on the image data and generates new recommended mirror positions. The WEx then invokes the MCS to plan commands and assure a safe move to the new positions. The WEx sends those commands to the Proposal Planning Subsystem (PPS) to attach to an Observatory visit, and the PPS includes that visit in the schedule it sends to the FOS for upload

to the Observatory. That visit includes taking confirmatory images, and the cycle repeats as the wavefront error is reduced.

The PM segments are controlled by hexapods which permit six rigid-body motions for each segment: piston, X and Y translation, X and Y tilt, and clocking. Since the global figure of the PM is rotationally-symmetric, tangential translation of a segment is degenerate with clocking, leaving five unique rigid-body motions. The Radius of Curvature (ROC) of each segment can be adjusted with a 7th actuator. The SM is also controlled by hexapod.

The PM and SM hexapod actuators each have a coarse and fine mechanism. The coarse mechanisms support length changes of several millimeters, with a step size of about 50 nm. When making coarse moves, the error is about 1% of the commanded move. The fine mechanism has a range of about 8 microns, with a step size of about 7 nm. When the fine mechanism reaches the end of its available travel, the coarse mechanism is automatically engaged, and the fine mechanism is set at the center of its range. Whenever the coarse mechanism is engaged, there is an additional 1-micron uncertainty in the length of the actuator. Consequently, the interplay between the coarse and fine mechanisms must be accounted for throughout the commissioning process.

The End-to-end WFSC commissioning process has been thoroughly tested in hardware using a scale model of the telescope [4], and through computer simulations, using the Integrate Telescope Model (ITM) [5]. The ITM uses an optical ray trace model of the telescope to generate the optical wavefront state of the telescope, and forms images after incorporating every known significant detail about the imaging process at each commissioning step. As such, the images are very realistic. The image data presented in the paper were generated with the ITM.

2. THE WFSC COMMISSIONING PROCESS

WFSC activities begin roughly 45 days after launch when the telescope has been deployed, and passively cooled to about 80 degrees K where the science instruments can begin to take images. Cooling continues throughout the commissioning process until it reaches its operating temperature, near 40 degrees Kelvin. The WFSC commissioning process has been designed with three guiding principles in mind:

- Correct the largest type of errors that are present at a given step.
- Consistently improve the alignment of the telescope (or decrease the wavefront error).
- Keep large moves of actuators to a minimum.

A high-level view of the WFSC commissioning process is shown in Figure 1. The process consists of three general phases of operations. In the first phase, segment location and positioning, we establish the approximate boresight of the telescope, and determine the rough pointing errors of each of the 18 segments. Images associated with each segment are identified and moved into a local image array for further wavefront analysis. In the second phase, we concentrate on eliminating the wavefront errors that exist locally within each segment. Large piston errors between the segments, segment-level power and astigmatism, and large field-dependent errors are corrected. In the third phase, we co-phase the individual segments relative to each other and correct any residual field-dependent wavefront errors. After correction of the field-dependent errors, the operation will loop back to one of three earlier points in the process, depending on the size of the multi-field errors that are corrected.

In the balance of this paper, we will describe the individual component processes in detail, presenting results from end-to-end commissioning simulations obtained through the ITM.

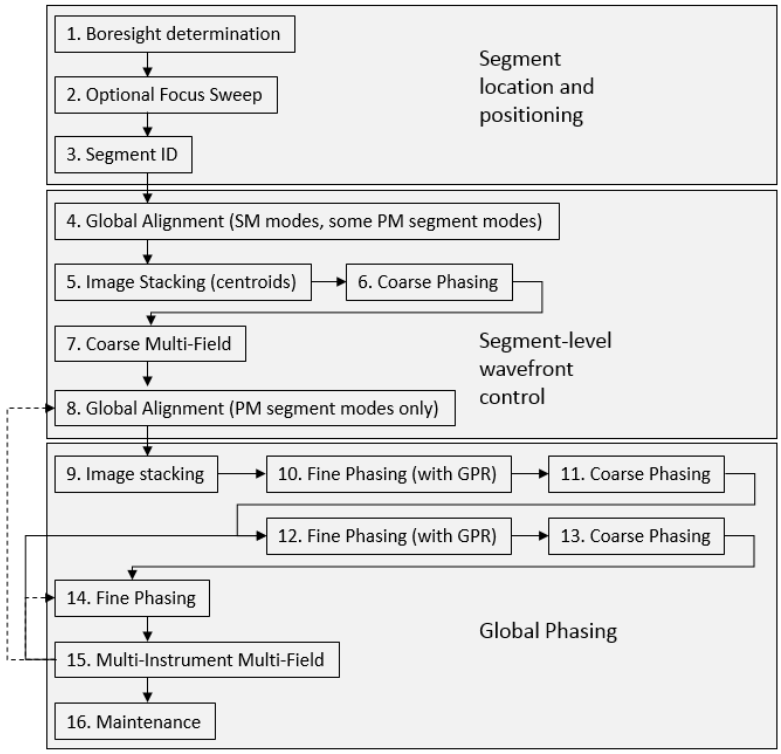

Figure 1. The WFSC commissioning process.

2.1 Image mosaic and boresight determination

When the telescope is deployed in space, it is anticipated that the PM segments will each be pointed at a different part of the sky, with the spread being approximately 10 arcminutes in diameter. There may also be an offset between the boresight defined by the average sky angle seen by the telescope, and that indicated by the spacecraft's star trackers. If this "boresight error" is modest—say, 15 arcminutes or less, we will point the telescope to a bright, isolated star and form an image mosaic covering that area, such as the one shown in Figure 2. In this case, the telescope boresight will simply be defined as the geometrical centroid of the 18 spots.

The problem of establishing the boresight becomes more difficult if the boresight error is significantly larger than 20 arcminutes. The number of images, downloads, observatory pointings, and the time required all increase with the square of the boresight error. Further, it becomes more difficult to find a bright star that is sufficiently isolated from neighboring stars. If this proves to be the case, we also have the option of pointing the telescope towards a moderately crowded star field and use a new cross-correlation technique [6] to establish the telescope boresight. There is some chance that not all 18 segment spots will be detected at this stage, in which case the missing segments will be located using the segment search process described below.

2.2 Focus sweep

The images obtained in the previous step may be significantly out of focus, owing to the inherent uncertainty of the deployment of the optics. A global focus error can be corrected by adjusting the SM in piston. The chief goal in the Focus Sweep is to obtain at least 1 image that is focused well enough to allow guiding with the Fine Guidance Sensor (FGS) [11] in subsequent steps. The SM will be scanned through focus, covering a range of approximately $\pm$400 microns, in five steps. An example of such a scan is shown in Figure 3. Our plan is to apply phase retrieval techniques [7] to the images from each visible segment to determine the focus error associated with that segment, and apply a SM piston correction that achieves the best global focus. However, even without

appealing to phase retrieval, it is obvious from Figure 3 that a correction of about +400 microns would result in a global improvement in focus.

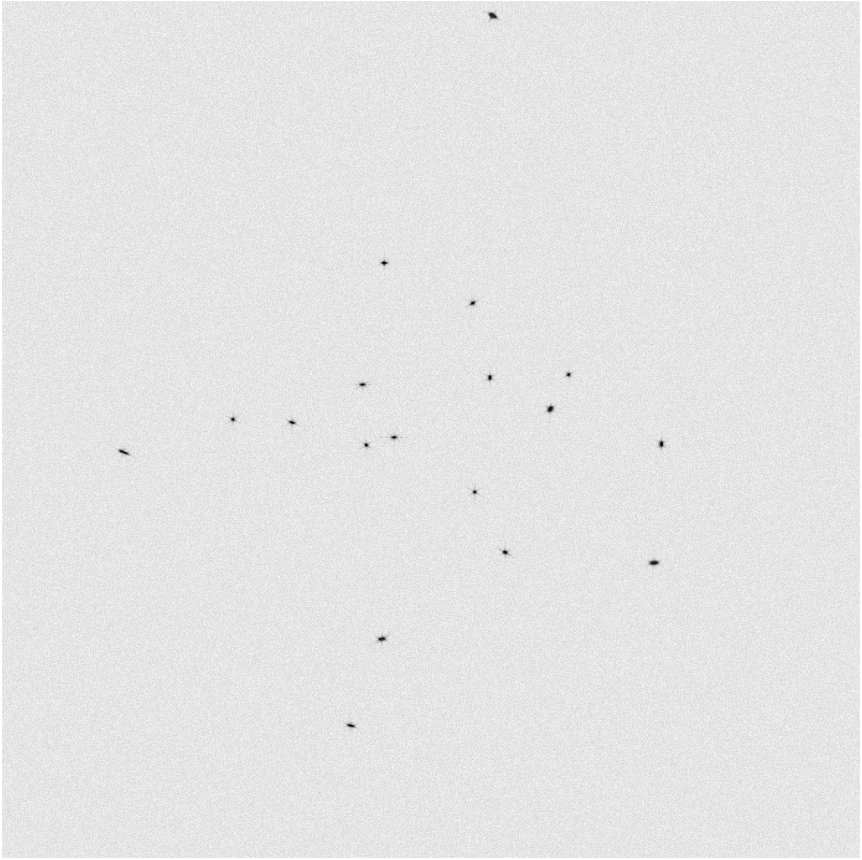

Figure 2. A simulated image mosaic (contrast inverted). The field of view is 25 arcminutes square.

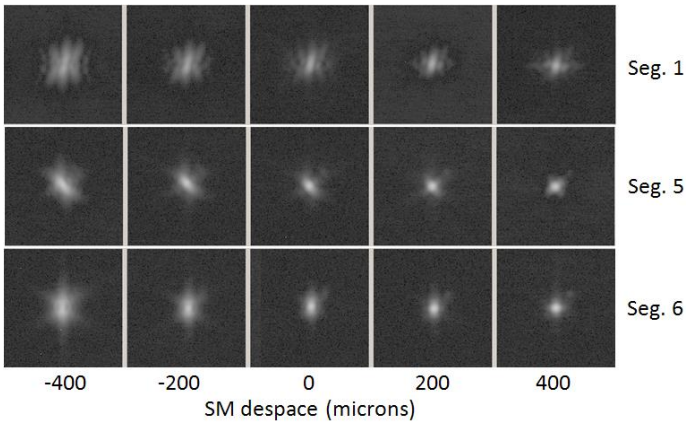

Figure 3. Scanning the SM through focus.

2.3 Segment ID

After ensuring that the telescope is reasonably in focus, the next step is to determine which segment corresponds to each image in the mosaic. We do this by carefully planning a series of telescope pointings so that all segment images are eventually imaged within NIRCam's field of view. At the first pointing location, all 18 segments are tilted a small amount, such that the corresponding segment image moves a few arcseconds across

the NIRCam focal plane. At each subsequent pointing location, segments identified during the previous operations are excluded. Images of the field are taken before and after tilting each segment. As shown in Figure 4, a simple differencing operation will reveal when a segment image has been moved. By carefully keeping track of the telescope pointing and the association between images and segment tilts, it will be possible to know the location of each segment image, relative to the established boresight.

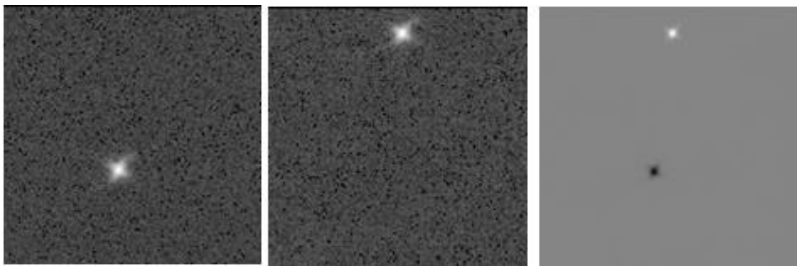

Figure 4. Before tilting segment (left), after tilting (center) and the differencing operation. Only a small portion of the field of view is shown here.

If the above process fails to identify all 18 segments, it is possible to search for a missing segment by issuing a series of segment tilt moves for the missing segment, in a spiral pattern, taking images before and after each move. For expediency, up to 200 moves can be queued up, images taken, and then analyzed, covering a field much larger than that offered by the NIRCam instruments.

After all 18 segments have been identified, PM segment tilts are issued to bring the segment images into a hexagonal array pattern, as illustrated in Figure 5-b. Since these are potentially large moves, we anticipate that there will be an unavoidable uncertainty of the image locations. Initially, the segments will be tilted so as to bring the associated images near the center of a single detector of one of NIRCam's 2x2 detector mosaics, giving us the maximum allowable margin for errors in the moves. Images are recorded before and after each segment move, so the segment images can be seen entering the science field, and identified. If a segment image misses the science field altogether, we will simply go back to a spiral search operation for that segment. After moving all segment images onto NIRCam's field of view, we will issue smaller and more precise moves to form the array.

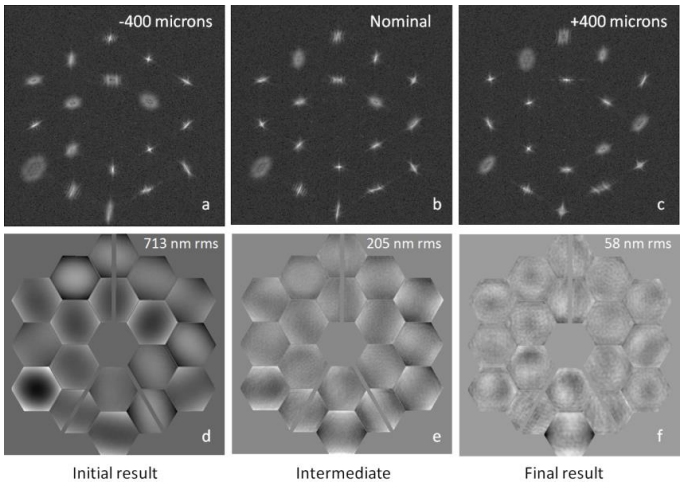

Figure 5. Top: image array at nominal and defocused SM position. Bottom, phase retrieval results.

2.4 Global alignment

With all 18 images in an array on NIRCam, we begin the process of eliminating the segment-level wavefront errors. Jitter-induced image blur can now be reduced by engaging the FGS of the spacecraft, which measures pointing errors at 15 Hz to drive a Fast Steering Mirror (FSM). One of the better segment images in the array is identified as a guide star (for example, the image in the 2 o'clock position in Figure 5) and the FGS loop is closed.

As in the case of the Focus Sweep, the SM is moved in piston to create defocused images. Because this piston motion will result in movement of the segment images, appropriate tip/tilt commands are also sent to each segment in order to retain each image's position in the array. A narrow-band filter in NIRCam centered at 2.12 microns is used in the imaging process, producing images such as those shown in Figure 5.

Each individual image is extracted from the larger 2048 X 2048 array and grouped with its counterpart(s) from the other focus positions. A phase retrieval algorithm is applied to each group of images to reconstruct the phase on the associated segment, removing the terms associated with tilting the segment into the array. The 18 resultant phase maps are stitched together to form the phase of the complete PM. Corrective moves are issued to the PM segments and the SM according to the phase results.

Global Alignment is executed at two different steps in the WFSC commissioning process, utilizing several iterations at each step. Each time Global alignment is invoked, wavefront errors appropriate for that step are corrected. Referring to Figure 1, Step 4 first invokes Global Alignment to correct segment level power. As shown in Figure 5-d, power is indeed the dominant term. The power is corrected locally by moving the segments in piston, and globally by moving the SM in piston.

After correcting the segment level power, another set of image data is acquired and analyzed to produce another wavefront. This is illustrated in Figure 5-e. Any remaining power in the segments will be corrected, along with the segment-level astigmatism, which is now dominant. Segment-level astigmatism can be partially reduced by applying small segment rotations about their normal axes (clocking).

The intermediate phase in Figure 5-e shows an indication of a pattern in the segment-level astigmatism. When there is strong indication of a global term, we may choose to correct the astigmatism first globally by translating or tilting the SM along its X and Y axes.

Global Alignment is invoked a second time (Step 8) after correcting any large piston errors that exist between the PM segments (via the Coarse Phasing process, Step 6), and any large multi-field errors (Step 7). Because those errors are assumed to have been corrected at this point, we do not make any further adjustments to the SM during the second Global Alignment. Segment-level power is corrected by adjusting the Radius of Curvature (ROC) actuators on the segments. Residual segment-level astigmatism is corrected again by a clocking adjustment, and finally by translating the segments radially with respect to the center of the PM. An example of the phase obtained after applying these corrections is shown in Figure 5-f. One segment (6 o'clock position) has residual astigmatism because correcting it would have required motions outside of the safety envelope established for that segment. All other segments show only residual coma and a bit of spherical aberration.

2.5 Image stacking

The purpose of Image Stacking is to move the individual segment images so that they fall precisely on top of each other at the center of the field, in preparation for Coarse Phasing. Sub-pixel stacking must be obtained, while the actuator fine mechanisms near the center of their dynamic range. Image stacking is performed 3 times. In the first operation, large piston errors will likely exist between the segments such that the stacked images will combine incoherently. In the next two operations, the piston errors will be much smaller and the stacked images will combine coherently. In the first case, therefore, we rely on image centroids to perform the stacking. In the second two operations, we rely on phase retrieval.

Stacking through centroids may appear superficially to be a simple process; however, it is complicated by four practical constraints:

- The accuracy of any large move of a segment is around 1%. Since we will be moving segment images from locations that are hundreds of pixels away from the stacking location, the best we could hope to do is to stack within a few pixels, where our goal is to stack within a fraction of a pixel. Iterative moves could be applied to precisely position each spot. However, once more than one spot is moved to the stack point, spot confusion results and the centroid of an unstacked spot cannot be determined. Therefore, the last move in stacking must be done blindly.
- In addition to the above uncertainty, movements of more than about 80 NIRCam pixels will cause the coarse mechanisms to be engaged on 1 or more actuators of a segment, resulting in about 1 micron of uncertainty in the length of the actuator.
- We must be careful to not use more than a small amount of the fine range in the stacking process, as it will be needed for subsequent steps. Consequently, the final stacking command must be issued in such a way as to leave the fine mechanisms near their centers.
- The Fine Guider System (FGS) needs to be active during the data acquisition. As the images are stacked, the segment images available for guiding become fewer. Consequently, the guide star must be changed, eventually guiding on the stacked images.

In the first image stacking process (step 5), we address the above constraints by stacking the images in 3 groups of 6. The first group of segments is tilted from their positions in the larger array to a smaller array to within about 40 pixels from the stack point. Images are taken before and after each move. Due to actuator uncertainties, the subset of spots will not end up in their desired locations; consequently, the centroid of each spot is measured and corrective moves are issued. The centroids are then measured again with the spots in this smaller array. This is illustrated in the Figure 6a.

Next, the spots are moved to the stack point using the coarse mechanisms, while intentionally recentering the fine mechanisms on all actuators. This recentering operation is followed by commands to move to spots back to their original locations in Figure 6a. However, because the fine mechanisms were recentered, errors in the resultant locations of the spots exist (Figure 6b). The centroids are remeasured and small corrective moves are issued, to reform the array as shown in Figure 6c.

Since the fine mechanisms were recentered when the spots were near the stack location, a final stack command will leave the fine mechanisms nearly centered, except for what is needed to correct for the uncertainty in the recentering process. The centroids are measured a final time, and the spots are moved to the stack point (Figure 6d).

The above process is repeated using 2 more groups of 6 segments. Before the final group of segments can be stacked, it is necessary to shift the guiding from one of the outer segments to the stacked group.

Image Stacking is used in Steps 5, 9 and 12, (Figure 1) as a precursor to Coarse Phasing. The first time Coarse Phasing is called, the goal is to merely reduce the large piston errors (~100 microns) between the segments to a few microns. Great accuracy is not needed, and therefore, the stacking does not have to be perfect. When Coarse Phasing is called again (Steps 11 and 13), we need the stacking accuracy to be as high as possible. Consequently, we use phase retrieval as implemented in the Fine Phasing step (Section 2.8 to measure and control any residual tip/tilt error among the segments.

The phase retrieval-based stacking process is simpler than the centroid-based process. 17 of the 18 segments are tilted from the large array to the stack point, leaving one spot unmoved for guiding. The actuators are commanded in a way such that the desired length is obtained while resulting in the centering of the fine mechanisms. Due to the previously discussed errors, the spots will fall scattered around the stack point by about

10 pixels rms, while demonstrating coherent interference. Images are taken at 6 different defocus positions (-8, -4, 0, +4, +8, +12 waves PTV at 2.12 microns). A Geometrical Phase Retrieval (GPR) algorithm [12] is applied to estimate the tip/tilt errors on the 17 segments to use as a starting estimate for the Fine Phasing algorithm. The phase retrieval algorithm robustly determines the corrective tip/tilt commands required to precisely stack the 17 images. As part of this correction, commands to bring in the 18th segment are issued, and the guiding is transferred to the stacked group. A few iterations of this process will nearly perfectly stack the images.

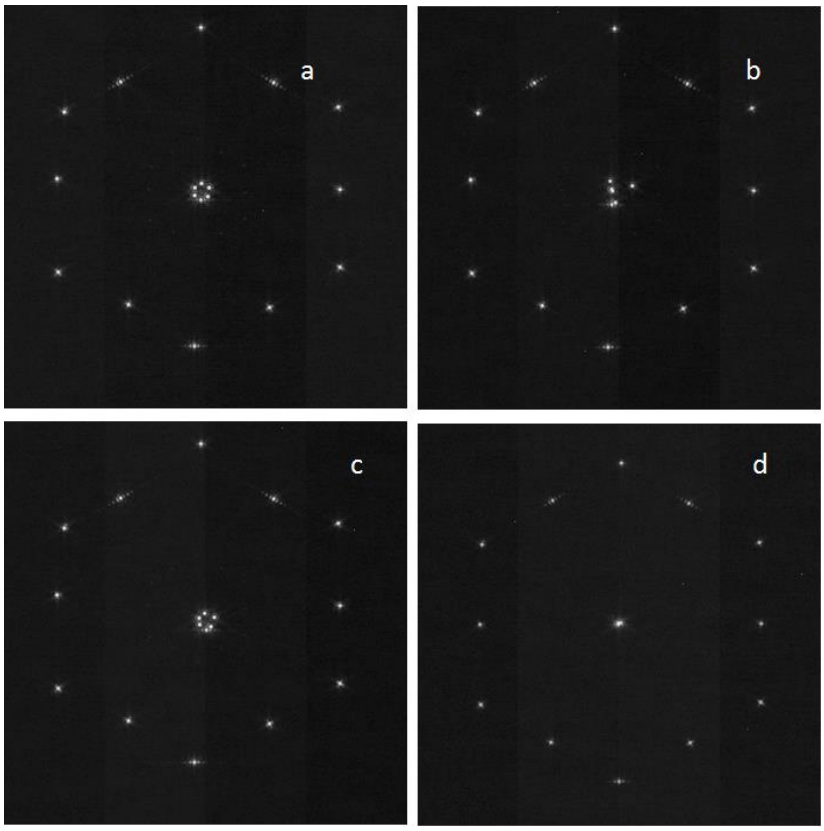

Figure 6. The centroid-based image stacking process. Stacking of the first group of 6 segments is illustrated. First, those segments are tilted into a small array (panel a), the fine mechanisms are recentered which causes some perturbations to the segment image positions (panel b), the small array is reformed (panel c) and finally small tilts move the segment images to the center (panel d).

2.6 Coarse phasing

Large piston errors between the individual segments are measured using a Dispersed Fringe Sensing (DFS) technique [8]. The principle behind the DFS operation is straightforward. Imagine an imaging system whose entrance aperture consists of two segments, with an unknown piston error between them. An image formed in monochromatic light has a characteristic shape that specifies the piston error, modulo 2π. An image formed at a slightly different wavelength would contain subtle differences, depending on the both the modulo value in the piston error, as well as the residual piston. With several wavelengths, it should be possible to determine the piston value exactly. The DFS technology uses a continuum of light which is dispersed across the detector. In the presence

of piston errors, the spectrum takes on the appearance of a barber-pole pattern, as shown in the top of Figure 7. By analyzing the "fringes" in this pattern, it is possible to determine the piston errors very accurately.

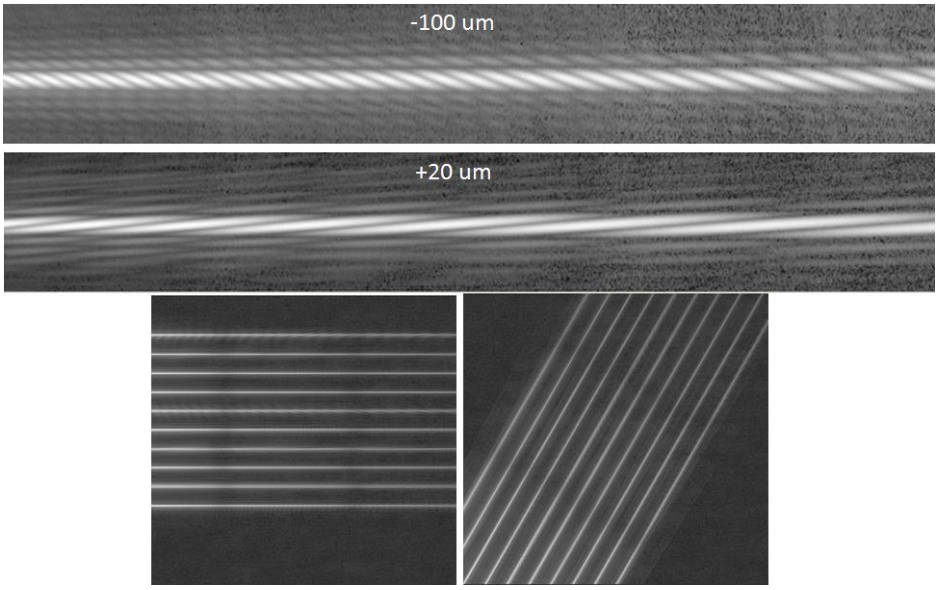

Figure 7. Top two rows: individual spectra from the coarse phasing process. Lower: DHS images.

The specific hardware used in the NIRCam instrument to form the spectra are known as Dispersed Hartmann Sensors (DHS). The DHS element is shown in the right of Figure 8. A subaperture mask is placed on an internal image of the pupil (or primary mirror) to form 10 individual pairs of subapertures (Figure 8). A grism placed after the mask provides the dispersion seen in the image. An additional prism is applied to each subaperture to shift the associated spectrum to a unique portion of the NIRCam detector. In NIRCam, two DHS elements are used to sample the piston differences which exist between 20 pairs of segments. Simulated images are shown in the bottom of Figure 7. One of the DHS elements is rotated 60 degrees. The two NIRCam modules use opposite rotation angles, to sample different segment pairs. Consequently, we can sample as many as 30 different segment pairs if needed.

As the piston errors are measured and corrected, the accuracy of the Coarse Phasing algorithm decreases, with the fringe separation increasing until no fringes are present. To avoid this effect, we always take DHS images before and after adding a small known piston offset (~3 microns) to some of the segments. The affected segments are shaded darker in Figure 8. Taken together, we are guaranteed to always have adequate signal for analysis.

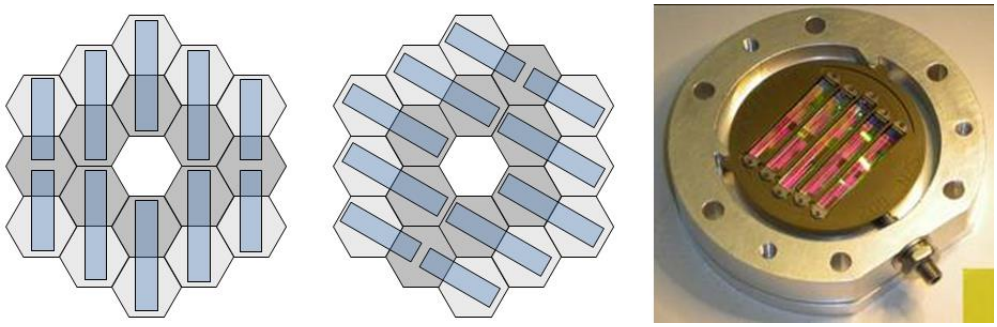

Figure 8. DHS subaperture (left and center). DHS flight hardware (right).

Once the piston values of all 20 subapertures are determined, a simple linear reconstruction algorithm is applied to determine the piston corrections for the 18 segments. Each subaperture can sense piston differences as large as about 350 microns. Beyond 350 microns, the fringe contrast becomes too small to analyze. With our current segment deployment uncertainties, we generally do not see piston errors this large. In the event that we encounter a piston value outside of the capture range, we can usually still determine all of the piston corrections, since the problem is slightly over-specified. If several subapertures produce fringes that cannot be analyzed, we can appeal to the second NIRCam channel for additional information. As a last resort, we can still reconstruct the piston solution in a piece-wise manner, which results in a piston discontinuity between otherwise phased sections of the PM segments. A scanning procedure is then applied to groups of segments until fringes are seen. Although scanning for fringes is a time-consuming process, it extends the potential capture range of Coarse Phasing to several millimeters of piston error, for use in a contingency mode.

Coarse Phasing is used three times in a nominal commissioning scenario. The first time it is invoked to measure and correct large piston errors, reducing them to about 5 microns per subaperture. The second time it is called, the residual errors are measured and reduced to near-zero values. In all likelihood, however, correction of these final piston values will result in engaging the coarse mechanisms on some of the segments, resulting in a potential 1-micron uncertainty on all affected actuators, and an average piston uncertainty of about 0.6 microns in the PM segments. Since Fine Phasing (Section 2.8) will be conducted at a wavelength of 2.12 microns, engaging coarse mechanisms could put us just outside of the Fine Phasing capture range, creating a 2π ambiguity in the final result. Consequently, Coarse Phasing is called a 3rd time for the purpose of sensing (and removing) the final small piston errors. Typically, all piston errors are reduced to less than about 250 nm.

2.7 Coarse multi-field sensing and control

After correction of the large piston errors and segment level wavefront errors, the dominant misalignment in the telescope will probably be an incorrect placement of the SM, resulting in a field-dependent error. We sense these errors by placing the segment images in a smaller version of the image array shown in Figure 5. By measuring relative centroids as this pattern is moved around to different field points of a single NIRCam channel, we can determine the SM positioning errors [10].

2.8 Fine phasing

The Fine Phasing operation is used to measure and correct small phasing errors between the PM segments. In general, this is only the tip, tilt and piston terms, although any type of correction could be applied if desired. Defocused images are taken in NIRCam using weak lenses placed in the filter and pupil wheels of each NIRCam module. There are a pair of lenses (+/- 8 waves) in the pupil wheels, and a single lens (+4 waves) in the filter wheel. Taken together, we can record images taken with -8, -4, 0, +4, +8, +12 waves PTV of defocus (at 2.12 microns wavelength) without having to change the nominal focus of NIRCam or of the telescope.

A phase retrieval algorithm [7] is applied to these defocused images to reconstruct the wavefront. An example of Fine Phasing is shown in Figure 9. These images were taken just before the last Coarse Phasing operation; hence, there is still a relatively large residual piston term on some of the segments. A second example is shown in Figure 10, which was obtained after the completion of the fine phasing process. In this result, the wavefront is 50 nm RMS, having corrected all but segment-level coma and spherical aberration.

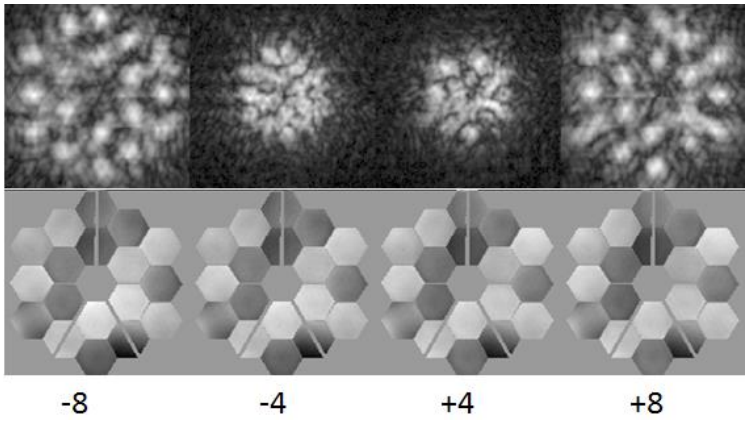

Figure 9. Fine phasing images and associated phase retrieval results. The PTV wavefront shown is 3 microns.

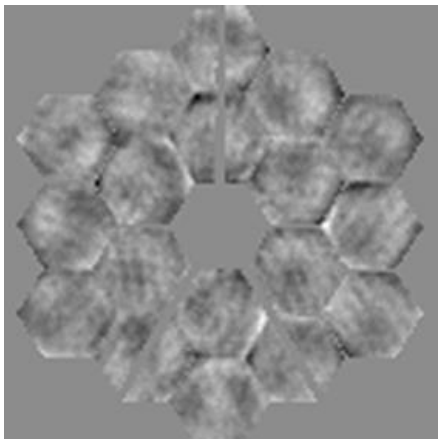

Figure 10. Final fine phasing result. The wavefront is 50 nm RMS.

2.9 Multi-instrument multi-field sensing and control

After completion of Fine Phasing, the telescope should be well-aligned, except for any field-dependent errors that were overlooked in the Coarse Multi-Field operation (Section 2.7). We record defocused images at 5 field points in each of the science instruments, using about $\pm$100 microns of SM piston to create the defocus. Phase Retrieval algorithms are applied to these images to determine the field-dependent wavefront errors.

Phase Retrieval on these images is more difficult [9] than that applied to NIRCam images for several reasons:

- The images are generally broad-band. (In the case of the Fine Guider instruments, the bandwidth is the entire near-IR spectrum.)
- The images are under-sampled for some wavelengths.
- In the case of the Near Infrared Spectrograph (NIRSpec), a micro-shutter array and an internal stop necessitate the use of a multiplane diffraction algorithm.
- The level of defocus is minimal, owing to the requirement to guide during the exposures. (Note that the images will also be defocused on the Fine Guider, and there is a limit to the amount of defocus that the FGS can accommodate.)

Working in favor of Phase Retrieval, however, is the fact that we will already know the fine details in the wavefront from the Fine Phasing result in NIRCam. Consequently, all that the Phase Retrieval algorithm will need to estimate is the power and astigmatism terms from the Multi-Field misalignment, and internal errors within each

instrument [10]. We do not currently plan on directly sensing the wavefront in NIRSpec as part of this process. However, we maintain the capability if it proves to be necessary.

2.10 Maintenance

At the completion of the commissioning process, Fine Phasing measurements will be automatically scheduled and processed every two days and analyzed to track the telescope alignment. The baseline plan is to apply a small correction to the telescope alignment as needed, approximately every two weeks. Maintenance operations will be the responsibility of the Space Telescope Science Institute.

3. REFERENCES

[1] T. Greene, C. Beichman, M. Gully-Santiago, D. Jaffe, D. Kelly, J. Krist, M. Rieke, and E. Smith, "NIRCam: development and testing of the JWST near-infrared camera," SPIE 7731, 77310C (2010).

[2] D. Swade, "Data management subsystem software architecture for JWST," SPIE 7737, 77371N (2010).

[3] T. Comeau and R. Whitman, "JWST wavefront sensing and controls software subsystem and executive requirements document," JWST-STSci-001202, SM-05.6, Rev B. (2011).

[4] D. S. Acton, T. Towell, J. Schwenker, D. Shields, E. Elliott, A. Contos, K. Hansen, F. Shi, B. Dean, J. S. Smith, "End-to-end commissioning demonstration of the James Webb Space Telescope," SPIE 6687, 668706 (2007)

[5] J., S. Knight, "Integrated telescope model for James Webb Space Telescope," SPIE, Vol. 8442, 84490V (2012).

[6] P. A. Lightsey, D. Scott Acton, J. Scott Knight, A. Contos, "James Webb Space Telescope first light boresight to spacecraft alignment determination," SPIE 8442, 84423H (2012).

[7] B. Dean, D. Aronstein, J. S. Smith, R. Shiri, D. S. Acton, "Phase retrieval algorithm for JWST flight and testbed telescope." SPIE, Vol. 6265, (2006).

[8] F. Shi, "Experimental verification of dispersed fringe sensing as a segment phasing technique using the Keck telescope," Applied Optics, Vol. 43, No10, p. 4474-4481, (2004).

[9] J. S. Smith, D. Aronstein, B. Dean, D. S. Acton, "Phase retrieval on broadband and under-sampled images for the JWST testbed telescope," SPIE 7436, 74360D (2009).

[10] D. Scott Acton and J. Scott Knight, "Multi-field alignment of the James Webb Space Telescope," SPIE Vol. 8442, 84423C (2012).

[11] R. Doyon, et al., "The JWST Fine Guidance Sensor (FGS) and Near-Infrared and Slitless Spectrograph(NIRISS), SPIE 8442, 84422R (2012).

[12] R. Elizabeth Carlisle and D. Scott Acton, "Demonstration of extended capture range for JWST phase retrieval," Appl. Opt. 54, 6454-6440 (2015).